

Energy shift and subharmonics induced by nonlinearity in a quantum dot system

Yuan Zhou(周圆), Gang Cao(曹刚), Hai-Ou Li(李海欧), and Guo-Ping Guo(郭国平)
Citation: Chin. Phys. B, 2023, 32 (**6**): 060303. DOI: 10.1088/1674-1056/acc521
Journal homepage: http://cpb.iphy.ac.cn; http://iopscience.iop.org/cpb

What follows is a list of articles you may be interested in

Electrical manipulation of a hole 'spin'-orbit qubit in nanowire quantum dot: The nontrivial magnetic field effects

Rui Li(李睿) and Hang Zhang(张航)
Chin. Phys. B, 2023, 32 (**3**): 030308. DOI: 10.1088/1674-1056/ac873b

High-fidelity universal quantum gates for hybrid systems via the practical photon scattering

Jun-Wen Luo(罗竣文) and Guan-Yu Wang(王冠玉)
Chin. Phys. B, 2023, 32 (**3**): 030303. DOI: 10.1088/1674-1056/ac8734

Steering quantum nonlocalities of quantum dot system suffering from decoherence

Huan Yang(杨欢), Ling-Ling Xing(邢玲玲), Zhi-Yong Ding(丁智勇), Gang Zhang(张刚), and Liu Ye(叶柳)
Chin. Phys. B, 2022, 31 (**9**): 090302. DOI: 10.1088/1674-1056/ac615a

Quantum speed limit of the double quantum dot in pure dephasing environment under measurement

Zhenyu Lin(林振宇), Tian Liu(刘天), Zongliang Li(李宗良), Yanhui Zhang(张延惠), and Kang Lan(蓝康)
Chin. Phys. B, 2022, 31 (**7**): 070307. DOI: 10.1088/1674-1056/ac4bd4

Self-error-rejecting multipartite entanglement purification for electron systems assisted by quantum-dot spins in optical microcavities

Yong-Ting Liu(刘永婷), Yi-Ming Wu(吴一鸣), and Fang-Fang Du(杜芳芳)
Chin. Phys. B, 2022, 31 (**5**): 050303. DOI: 10.1088/1674-1056/ac4489

Energy shift and subharmonics induced by nonlinearity in a quantum dot system

Yuan Zhou(周圆)[1,2], Gang Cao(曹刚)[1,2], Hai-Ou Li(李海欧)[1,2,†], and Guo-Ping Guo(郭国平)[1,2,3]

[1] *CAS Key Laboratory of Quantum Information, University of Science and Technology of China, Hefei* 230026, *China*
[2] *CAS Center For Excellence in Quantum Information and Quantum Physics, University of Science and Technology of China, Hefei* 230026, *China*
[3] *Origin Quantum Computing Company Limited, Hefei* 230026, *China*

(Received 13 February 2023; revised manuscript received 8 March 2023; accepted manuscript online 17 March 2023)

The presence of anticrossings induced by coupling between two states causes curvature in energy levels, yielding a nonlinearity in the quantum system. When the system is driven back and forth along the bending energy levels, subharmonic transitions and energy shifts can be observed, which would cause a significant influence as the system is applied to quantum computing. In this paper, we study a longitudinally driven singlet-triplet (ST) system in a double quantum dot (DQD) system, and illustrate the consequences of nonlinearity by driving the system close to the anticrossings. We provide a straightforward theory to quantitatively describe the energy shift and subharmonics caused by nonlinearity, and find good agreement between our theoretical result and the numerical simulation. Our results reveal the existence of nonlinearity in the vicinity of anticrossings and provide a direct way of analytically assessing its impact, which can be applied to other quantum systems without excessive labor.

Keywords: quantum dot, quantum computing, nonlinear physics

PACS: 03.67.Lx, 03.67.–a, 68.65.Hb, 78.47.jh **DOI:** 10.1088/1674-1056/acc521

1. Introduction

Nonlinearity has been extensively explored especially in modern photonic functionalities, including laser light control, generation of ultrashort pulses, all-optical signal processing, *et al.*[1,2] It also plays an important role in superconducting circuits[3] and other emerging systems such as graphene,[4] plasmonics,[5,6] and nanomechanicals.[7–9] In gate-defined quantum dot (QD) system,[10–15] the subharmonics caused by nonlinearity have also been observed.[16–20] One mechanism that leads to nonlinearity in the QD system is the appearance of nonlinear dependence of electric g-tensor on the applied field.[21,22] Moreover, the nonlinearity can also be introduced by anharmonic confining potential,[19,23] orbital dynamics,[24] and Landau–Zener–Stückelberg (LZS) dynamics.[18,25] Magnetic misalignment and Rashba spin–orbit coupling are also probable mechanisms[26] that lead to nonlinearity in QD.

Aside from the above mechanisms, nonlinearity can also be introduced when the system is driven in the vicinity of the anticrossing, and the nonlinearity can be significant when the system is close to the anticrossing. As we would show later, this kind of nonlinearity is caused by the curving energy levels near the anticrossings in essence, and thus is not limited to the QD system. More importantly, the resulting driving-dependent energy shift is crucial for high-fidelity qubit control.[27] Meanwhile, subharmonic transitions can be employed to simplify microwave engineering in qubit control.[19]

In this work, we study the nonlinearity by focusing on the regime where the system experiences a longitudinal drive near the anticrossings, while keeping the driving amplitude small enough to avoid the system passing through the anticrossings. We demonstrate our results based on the ST system in a DQD, which is one of the most studied quantum systems consisting of two spins.[28–33] Based on the ST system, we observe the driving-dependent Bloch–Siegert shift[34] and the subharmonic transitions in its spectrum. We find that the resonant frequency shifts with both energy detuning and driving amplitude, which can be of great importance in high-fidelity qubit control.[27] Moreover, we study the non-linear dependency of the Rabi frequencies on driving amplitude in both principal and subharmonics, which suggests the potential application of the subharmonics in qubit control.[19] The mechanism of nonlinearity we study here can coexist with other mechanisms and is not limited to QDs; thus, it is versatile and of unignorable significance to other systems.

2. Results

The ST systems have attracted much attention in recent years due to their intriguing energy structure, enriched phenomena, convenient readout, and most importantly, demonstration of spin-based two-qubit gates.[28–33] The ST system consists of two spins in a coupled DQD system, and the lowest five energy levels are relatively isolated from other excited states. The basis of the five-level subspace can be given by $\{|\uparrow\uparrow\rangle, |\uparrow\downarrow\rangle, |\downarrow\uparrow\rangle, |\downarrow\downarrow\rangle, |S_{20}\rangle\}$, in which the arrows represent

†Corresponding author. E-mail: haiouli@ustc.edu.cn

© 2023 Chinese Physical Society and IOP Publishing Ltd

the spin states and S represents the singlet state. The charge configurations of the first four states are the same, given by $|(1,1)\rangle$, which means one spin in each dot, while the configuration of $|S_{20}\rangle$ is $|(2,0)\rangle$, which means both spins are located in the left dot.

Supposing the g-factors are scalars, i.e., g_1 and g_2, the dynamics of the ST system can be described by the following Hamiltonian:[28,29,35,36]

$$\boldsymbol{H}_5 = \begin{pmatrix} \bar{E}_z & 0 & 0 & 0 & t_{\rm so} \\ 0 & \delta E_z & 0 & 0 & t/\sqrt{2} \\ 0 & 0 & -\delta E_z & 0 & -t/\sqrt{2} \\ 0 & 0 & 0 & -\bar{E}_z & t_{\rm so} \\ t_{\rm so} & t/\sqrt{2} & -t/\sqrt{2} & t_{\rm so} & \varepsilon \end{pmatrix}, \tag{1}$$

where $\bar{E}_z = (g_1+g_2)\mu_{\rm B}B/2$, $\delta E_z = (g_1-g_2)\mu_{\rm B}B/2$, with B being the magnetic field strength, $\mu_{\rm B}$ being the Bohr magneton, and ε being the energy detuning between two QDs. The off-diagonal elements t and $t_{\rm so}$ are the tunnel coupling and spin–orbit coupling strengths, respectively. In the following discussion, we set $g_1 = 4.0$, $g_2 = 3.0$, and $t_{\rm so} = 5$ μeV, $t = 16$ μeV, which is accessible in the experiment.[35–37] In practice, detuning ε can be relevant to gate geometry though,[10] it is often tuned by gate voltages. Anticrossings can be found when $\varepsilon \approx 0$ in the ST system, which plays an important role in state manipulation.[12,13] The energy levels as a function of detuning ε with $B = 0.25$ T is presented in Fig. 1 by solid lines. From the spectrum, we see the energy levels bend in the neighbor of anticrossings, which implies the existence of nonlinearity and leads to higher harmonics of the driving field. Obviously, the closer the system is to the anticrossings, the more significant the nonlinearity is.

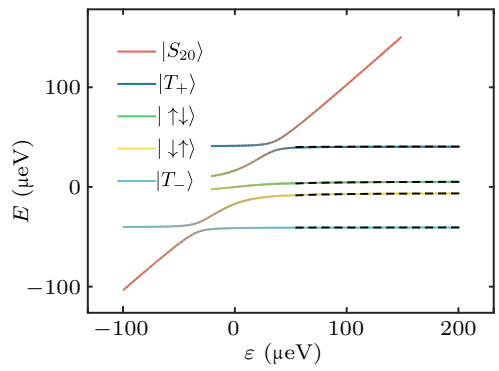


Fig. 1. Energy levels versus detuning ε. The energy levels given by Eq. (1) are presented as solid lines, while the results of Eq. (2) are given by black dashed lines. The energy levels are calculated with $g_1 = 4.0$, $g_2 = 3.0$, $t_{\rm so} = 5$ μeV, $t = 16$ μeV, and $B = 0.25$ T. In the vicinity of anticrossing, we can see a non-linear dependency of the energies on detuning ε.

In the matrix form of the Hamiltonian given in Eq. (1), the nonlinearity is not obvious. The curving energy levels suggest that the mechanism of nonlinearity originates from the couplings, in other words, perturbation from $|S_{20}\rangle$. In addition, in the context of spin two-qubit gates, we are interested in the transitions between two-qubit product states, i.e., $|\uparrow\uparrow\rangle, |\uparrow\downarrow\rangle, |\downarrow\uparrow\rangle, |\downarrow\downarrow\rangle$. Hence, we suppose the detuning ε is large enough ($\varepsilon \gg t_{\rm (so)}$) and treat $|S_{20}\rangle$ perturbatively by a Schrieffer–Wolff (SW) method.[38,39] After SW transformation, we obtain a 4×4 Hamiltonian as follows:

$$\boldsymbol{H}_4 = \begin{pmatrix} \bar{E}_z + J_{\rm so} & \Delta & -\Delta & J_{\rm so} \\ \Delta & \delta E_z + J_t & -J_t & \Delta \\ -\Delta & -J_t & -\delta E_z + J_t & -\Delta \\ J_{\rm so} & \Delta & -\Delta & -\bar{E}_z + J_{\rm so} \end{pmatrix}, \tag{2}$$

where

$$J_{\rm so} \approx \frac{t_{\rm so}^2}{\varepsilon},\ J_t \approx \frac{t^2}{2\varepsilon},\ \Delta \approx \frac{t\times t_{\rm so}}{\sqrt{2}\varepsilon}. \tag{3}$$

Notice that in Eq. (3), we neglect the contribution of $\pm\bar{E}_z$ and $\pm\delta E_z$ in J_t, $J_{\rm so}$, Δ by assuming $\varepsilon \gg \bar{E}_z$, δE_z, and make an approximation $1/(\pm\bar{E}_z+\varepsilon) \approx 1/(\pm\delta E_z+\varepsilon) \approx 1/\varepsilon$. The energy levels calculated by H_4 are also presented in Fig. 1 by the dashed lines, and we find good agreement between the two results from the comparison, which illustrates the accuracy of the perturbation. In Eq. (2), we see that perturbation-induced terms J_t, $J_{\rm so}$, and Δ all depend on ε non-linearly, and the curving energy levels can be well described. In addition, the nonlinear dependency on ε reminds us that by applying a drive to ε, i.e., $\varepsilon = \varepsilon_0 + \varepsilon_1\sin(2\pi ft)$ (ε_1 represents the driving amplitude and ε_0 determines the working point), we would obtain higher-harmonics of driving frequency f and observe subharmonic transitions between either two product states. However, SW transformation cannot be simply applied since the Hamiltonian matrix is now time-dependent. Fortunately, the influence of the time-dependent term is on the order of $\mathcal{O}(hf\varepsilon_1/\varepsilon_0^2)$, where h is the Plank constant. To eliminate this problem, we restrict ourselves to the condition that ε_1 and f are small enough compared to ε_0, i.e., $hf\varepsilon_1 \ll \varepsilon_0^2$, which is reasonable in practice, so that Eq. (2) is still valid when ε is time dependent. In general, the nonlinearity is significant when close to the anticrossings, but we shall avoid the system passing through the anticrossings, where the SW transformation fails. For problems beyond our discussion, e.g., $\varepsilon_1 \geq \varepsilon_0$, one can turn to a more versatile but sophisticated approach.[25,40–42]

When a driving field is applied, according to Eq. (3), we have $\Delta = t\times t_{\rm so}/(\sqrt{2}(\varepsilon_0+\varepsilon_1\sin(2\pi ft)))$. For ε_1 is small compared to ε_0, Δ can be expanded as follows:

$$\Delta(t) = \frac{1}{\sqrt{2}\varepsilon_0}\sum_{n=0}(-1)^n\left(\frac{\varepsilon_1}{\varepsilon_0}\sin(2\pi ft)\right)^n. \tag{4}$$

This equation indicates the existence of higher harmonics of f in Δ. We perform a Fourier transformation of Δ in the condition of $\varepsilon_0 = 200$ μeV, $\varepsilon_1 = 100$ μeV, and the resulting $\mathcal{F}(\Delta)$ is presented in Fig. 2(a). From $\mathcal{F}(\Delta)$ we clearly see the higher harmonics of Δ labeled by $\Delta^{(n)}$, $n = 1,\ldots,4$. Furthermore, we track the value of $\Delta^{(n)}$ as the driving amplitude varies, and the results are presented in Fig. 2(b) by the solid lines. When

the amplitude ramps up, the subharmonics become more significant. To observe the nonlinearity induced by the curving energy levels, we calculate the time-averaged transition probability between $|\uparrow\uparrow\rangle \leftrightarrow |\uparrow\downarrow\rangle$ (labeled by T_{12}) and $|\downarrow\uparrow\rangle \leftrightarrow |\downarrow\downarrow\rangle$ (labeled by T_{34}), which is defined by

$$T_{ij} = \lim_{t\to\infty} \frac{1}{t} \int_0^t |\langle i|U(\tau,0)|j\rangle|^2 \mathrm{d}\tau, \tag{5}$$

where $U(\tau,0)$ is the time-evolution operator from time $t=0$ to $t=\tau$. The numerical simulation is carried out based on the Floquet method[43] by substituting $\varepsilon = \varepsilon_0 + \varepsilon_1 \sin(2\pi f t)$ to Eq. (1). From Fig. 2(b) we see that when $\varepsilon_1 = 100$ μeV, the subharmonics are considerable; thus, the subharmonic transitions are supposed to be obvious. In Fig. 2(c), we present the transition probability $T_{12}+T_{13}$ as a function of driving frequency f and external magnetic field strength B when $\varepsilon_1 =$ 100 μeV. From this result we clearly see two principal transitions, which represent manipulation of spin on the right (T_{12}) and left (T_{13}) dots, respectively. In addition, subharmonics are also observed as expected, which is generated by the nonlinearity included in the energy levels. With respect to the appearance of subharmonics induced by the nonlinearity, there are two subsequent problems we are interested in, i.e., (i) how are the resonant frequencies and (ii) Rabi frequency influenced by the driving field? In what follows, we study these two questions both numerically and theoretically.

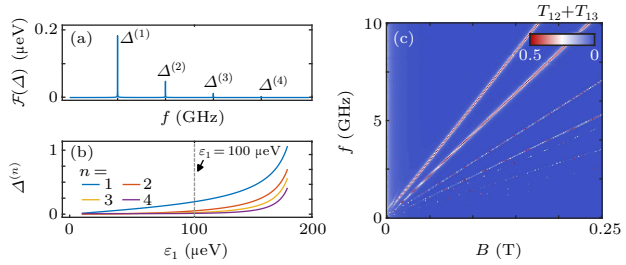


Fig. 2. Higher harmonics of driving frequency included in Δ. (a) Fourier transformation of $\Delta(t)$, in which higher harmonics $\Delta^{(n)}$, $n = 1,\ldots,4$ are obvious. (b) $\Delta^{(n)}$ versus driving amplitude ε_1. When ε_1 increases, the subharmonics become more significant. (c) Transition probability $T_{12}+T_{13}$ as a function of driving frequency f and magnetic field strength B. The simulation is carried out by setting $\varepsilon_0 = 200$ μeV and $\varepsilon_1 = 100$ μeV, as indicated by the vertical dashed line in panel (b). Both principal and subharmonics are observed, which is in good agreement with the theoretical prediction.

First, we investigate how the resonant frequency depends on the ε_0 and ε_1. According to Eq. (3), we learn that $J_{t,\mathrm{so}} \propto (\varepsilon_0 + \varepsilon_1 \sin(2\pi f t))^{-1}$. Note that in the condition of $\varepsilon_0 > \varepsilon_1$, we have

$$\frac{1}{T}\int_0^T \frac{1}{\varepsilon_0 + \varepsilon_1 \sin(\frac{2\pi}{T}t)} \mathrm{d}t = \frac{1}{\sqrt{\varepsilon_0^2 - \varepsilon_1^2}}, \tag{6}$$

which indicates that the mean values of $J_{t,\mathrm{so}}$ are not zero. We denote the net contributions as $\overline{J_{t,\mathrm{so}}}$, which are dependent on both ε_0 and ε_1, and determine the resonant frequency. This kind of frequency shift generated by the longitudinal drive is called the Bloch–Siegert shift,[34] which can be well described by the Floquet method,[43] whereas we can interpret it in a more straightforward way in the language of nonlinearity here.

To illustrate the energy shift induced by the nonlinearity, we calculate the averaged transition probability $|\uparrow\uparrow\rangle \leftrightarrow |\downarrow\uparrow\rangle$ (T_{13}) and $|\uparrow\downarrow\rangle \leftrightarrow |\downarrow\downarrow\rangle$ (T_{24}). These two transitions are closely watched in the experiment since they are relevant to the two-qubit controlled-NOT gate.[29,33,44] The simulation is carried out with $B = 0.1$ T, and the joint probability $T_{13}+T_{24}$ is presented in Figs. 3(a) and 3(b). To be specific, simulation in Fig. 3(a) is carried out with $\varepsilon_1 = 50$ μeV, while in Fig. 3(b) we set $\varepsilon_0 = 800$ μeV. As we can see, the resonant frequencies shift along with ε_0 and ε_1 in Figs. 3(a) and 3(b), respectively. To quantitatively study the energy shift, we extract the distance between two transition peaks from Figs. 3(a) and 3(b), and the results are presented by the scatters in Figs. 3(c) and 3(d). From Eq. (2), this energy difference can be described by $\delta f = 2\times\overline{J_t - J_{\mathrm{so}}}$. We present the result of $\delta f = 2\times\overline{J_t - J_{\mathrm{so}}}$ in Figs. 3(c) and 3(d) with solid lines, while the dashed lines in yellow and purple stand for the contributions from $\overline{J_t}$ and $\overline{J_{\mathrm{so}}}$, respectively. We find good agreement between the simulation and theory from Figs. 3(c) and 3(d), which proves that the energy shift can be explained by the nonlinearity here. Furthermore, the ε_0-dependent δf can be directly interpreted from the energy structure of ST in Fig. 1, nonetheless, the ε_1-dependency of δf is non-trivial, which is relevant to the nonlinearity. Based on the fact that energy shift plays an important role in achieving high-fidelity qubit control,[27] the nonlinearity we study here is crucial in realizing a high-fidelity controlled-NOT gate.

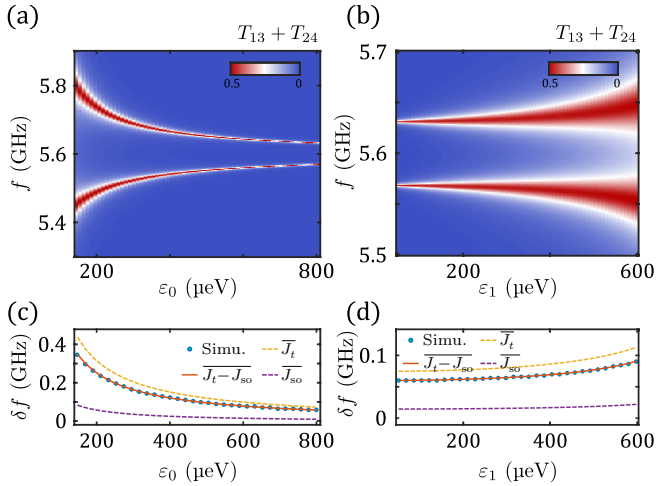


Fig. 3. Bloch–Siegert shift induced by nonlinearity. (a) Transition probabilities $T_{13}+T_{24}$ as a function of driving frequency f and ε_0 with $\varepsilon_1 = 50$ μeV. (b) $T_{13}+T_{24}$ as a function of f and ε_1 with $\varepsilon_0 = 800$ μeV. From the results we see that the resonant transitions shift with ε_0 and ε_1. Panels (c) and (d) are frequency differences δf between two transitions versus ε_0 (c) and ε_1 (d). The results extracted from the simulation are presented by the scatters, and the theoretical results are indicated by lines. The energy shift can be well described by $2\times\overline{J_t - J_{\mathrm{so}}}$, which agrees well with the theory.

In addition to the energy shift, we also observe a change in the linewidth of the resonant signal in Fig. 3. Since dissipation is not included in the simulation, the linewidth of T_{ij} directly indicates the Rabi frequency of the relevant resonance. To this end, we study the Rabi frequency between different product states as a function of driving amplitude. Higher harmonics of the driving frequency are induced by the nonlinearity included in the energy levels, which can be described by Eq. (2). As aforementioned, the net contribution of diagonal terms $J_{t,\mathrm{so}}$ dominates the energy shift. In the following, we investigate the influence of off-diagonal terms on the Rabi frequency. Before focusing on the subharmonics, we evaluate the influence of the time-independent part of the off-diagonal terms, i.e., the mean values of Δ and $J_{t,\mathrm{so}}$. As we discussed above, $J_{t,\mathrm{so}}$ has a nonzero mean value, as does Δ. According to Eq. (6), the value of the time-independent part is on the order of ε_0^{-1}, which is sufficiently small compared to the driving frequency. Hence, the influence of the time-independent off-diagonal terms can be neglected during rotating wave approximation (RWA).

Since all the states are directly connected to each other by matrix elements in Eq. (2), we expect resonant transitions between either two product states. We calculate the averaged transition probability of $|\uparrow\uparrow\rangle \leftrightarrow |\uparrow\downarrow\rangle$ (T_{12}), $|\uparrow\downarrow\rangle \leftrightarrow |\downarrow\uparrow\rangle$ (T_{23}) and $|\uparrow\uparrow\rangle \leftrightarrow |\downarrow\downarrow\rangle$ (T_{14}) with $B = 0.1$ T, $\varepsilon_0 = 400$ μeV, where T_{12} represents the flip of a single spin, T_{12} is for the two-qubit SWAP, and T_{14} is for two spins flip simultaneously. Here, we extract the Rabi frequency f_{rabi} of each process at both principal and second-order harmonics, and show the dependency of f_{rabi} on driving amplitude ε_1, which ranges from 50 μeV to 300 μeV. The system can be described by a two-level model when it is on resonance; thus, we can obtain f_{rabi} from the width of the time-averaged transition peaks. The theoretical result can also be obtained without excessive labor, i.e., the f_{rabi} is determined by the Fourier components of the corresponding off-diagonal terms.

The Rabi frequency for each process labeled by f_{12}, f_{23}, and f_{14} under different driving amplitudes ε_1 is presented by scatters in Fig. 4. For the principal ($n = 1$) and second harmonic ($n = 2$), f_{rabi} depends differently on ε_1, as shown in Figs. 4(a) and 4(b). Specifically, for $n = 1$, $f_{\mathrm{rabi}} \propto \varepsilon_1^1$ when ε_1 is relatively small. When ε_1 increases, the second harmonic becomes significant, and the dependency is non-linear and is more like $f_{\mathrm{rabi}} \propto \varepsilon_1^2$. For $n = 2$, the relationship is entirely nonlinear, given by $f_{\mathrm{rabi}} \propto \varepsilon_1^2$ and $f_{\mathrm{rabi}} \propto \varepsilon_1^3$ for small and great driving amplitudes, respectively. The theoretical results are also presented in Figs. 4(a) and 4(b) by solid lines, which is in accordance with the simulation. This result shows that, when the driving amplitude is small, we have $f_{\mathrm{rabi}} \propto \varepsilon_1^n$ for n_{th}-order harmonics, which is in accordance with the experiment.[19] When ε_1 becomes greater, the expansion in Eq. (4) is inaccurate, and a higher harmonic dominates the dynamics. Even so, the Fourier coefficient of the coupling elements is able to describe this result correctly in the whole range. This result also indicates the potential of subharmonics in qubit control[19] since driving a qubit at half of its Larmor frequency would substantially lower the requirement in microwave engineering. Regarding the decoherence rate, it has a positive correlation with the derivative of energy levels about ε_0 and may be dependent on temperature.[45,46] Thus, in order to perform qubit control based on subharmonics, the working point and driving amplitude should be carefully chosen, and the parameter optimization is left for future experiments.

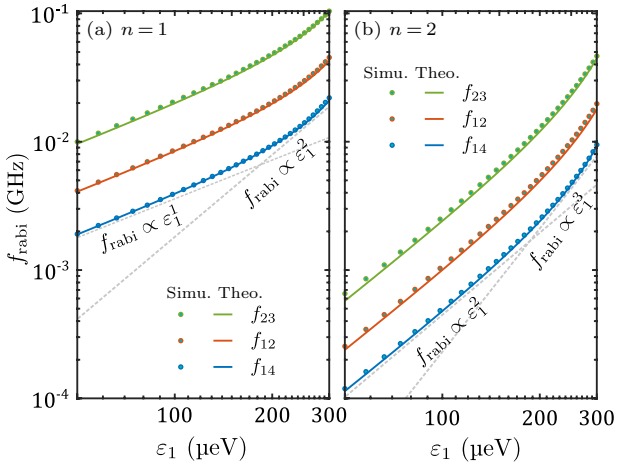


Fig. 4. Rabi frequencies f_{12}, f_{23}, and f_{14} (extracted from T_{12}, T_{23}, and T_{14}) versus ε_1 at the principal (a) and second harmonic (b). The results from numerical simulation are presented by scatters, while the results from theory are displayed by lines. The gray dashed guiding lines are also placed in panels (a) and (b), which represent $f_{\mathrm{rabi}} \propto \varepsilon_1^1$, $f_{\mathrm{rabi}} \propto \varepsilon_1^2$, and $f_{\mathrm{rabi}} \propto \varepsilon_1^3$.

3. Conclusion

We study the nonlinearity introduced by the bending energy levels of an ST system in a DQD, which can be found near the anticrossings. By applying a longitudinal drive near the anticrossings, we demonstrate the energy shift and subharmonic transitions induced by the nonlinearity. In the context of quantum computing, the driving-dependent energy shift can be important with respect to high-fidelity qubit control,[27] and the subharmonic transitions can be potentially helpful to lower the requirement of microwave engineering.[19] In the regime of $\varepsilon_0 > \varepsilon_1 \gg t_{\mathrm{so}}, t, f$, we provide a concise approach to quantitatively describe the nonlinearity and its corresponding phenomena. To be specific, by applying SW transformation, we obtain a reduced Hamiltonian, in which the matrix elements depend on ε non-linearly. In this way, the energy shifts are well described by the mean values of the diagonal elements, and the higher harmonics are generated from the harmonics of the off-diagonal elements. This understanding of the nonlinearity is intuitive, convenient, and comprehensive and is essential to high-fidelity qubit manipulation. Last, the mechanism of non-

linearity we introduced here is not limited to the QD systems and, thus, our results can be important to other quantum systems.

Acknowledgments

Project supported by the National Natural Science Foundation of China (Grant Nos. 12074368, 92165207, 12034018 and 92265113), the Anhui Province Natural Science Foundation (Grant No. 2108085J03), and the USTC Tang Scholarship.

References

[1] Scully M O and Zubairy M S 1997 *Quantum Optics* (Cambridge: Cambridge University Press)
[2] Boyd R 2003 *Nonlinear Optics* (Elsevier Inc.)
[3] Krantz P, Kjaergaard M, Yan F, Orlando T P, Gustavsson S and Oliver W D 2019 *Appl. Phys. Rev.* **6** 021318
[4] Hendry E, Hale P J, Moger J, Savchenko A K and Mikhailov S A 2010 *Phys. Rev. Lett.* **105** 097401
[5] Maier S A and Atwater H A 2005 *J. Appl. Phys.* **98** 011101
[6] Kauranen M and Zayats A 2012 *Nat. Photonics* **6** 737
[7] Kacem N, Hentz S, Pinto D, Reig B and Nguyen V 2009 *Nanotechnology* **20** 275501
[8] Su Z J, Ying Y, Song X X, Zhang Z Z, Zhang Q H, Cao G, Li H O, Guo G C and Guo G P 2021 *Nanotechnology* **32** 155203
[9] Bachtold A, Moser J and Dykman M 2022 *Rev. Mod. Phys.* **94** 045005
[10] Zhou C, Wang L, Tu T, Han T Y, Li H O and Guo G P 2013 *Chin. Phys. Lett.* **30** 050301
[11] Chen B, Wang B, Cao G, Li H, Xiao M and Guo G 2017 *Sci. Bull.* **62** 712
[12] Zhang X, Li H O, Wang K, Cao G, Xiao M and Guo G P 2018 *Chin. Phys. B* **27** 020305
[13] Zhang X, Li H O, Cao G, Xiao M, Guo G C and Guo G P 2019 *Natl. Sci. Rev.* **6** 32
[14] Wang K, Li H O, Xiao M, Cao G and Guo G P 2018 *Chin. Phys. B* **27** 090308
[15] Xu Y Q, Gu S S, Lin T, Wang B C, Li H O, Cao G and Guo G P 2023 *Sci. China: Phys., Mech. Astron.* **66** 237301
[16] Laird E A, Barthel C, Rashba E I, Marcus C M, Hanson M P and Gossard A C 2009 *Semicond. Sci. Technol.* **24** 064004
[17] Schroer M D, Petersson K D, Jung M and Petta J R 2011 *Phys. Rev. Lett.* **107** 176811
[18] Stehlik J, Schroer M D, Maialle M Z, Degani M H and Petta J R 2014 *Phys. Rev. Lett.* **112** 227601
[19] Scarlino P, Kawakami E, Ward D R, Savage D E, Lagally M G, Friesen M, Coppersmith S N, Eriksson M A and Vandersypen L M 2015 *Phys. Rev. Lett.* **115** 106802
[20] Forster F, Mühlbacher M, Schuh D, Wegscheider W and Ludwig S 2015 *Phys. Rev. B* **91** 195417
[21] De A, Pryor C E and Flatté M E 2009 *Phys. Rev. Lett.* **102** 017603
[22] Pingenot J, Pryor C E and Flatté M E 2011 *Phys. Rev. B* **84** 195403
[23] Scarlino P, Kawakami E, Jullien T, Ward D R, Savage D E, Lagally M G, Friesen M, Coppersmith S N, Eriksson M A and Vandersypen L M 2017 *Phys. Rev. B* **95** 165429
[24] Rashba E I 2011 *Phys. Rev. B* **84** 241305
[25] Danon J and Rudner M S 2014 *Phys. Rev. Lett.* **113** 247002
[26] Romhányi J, Burkard G and Pályi A 2015 *Phys. Rev. B* **92** 054422
[27] Yoneda J, Takeda K, Otsuka T, Nakajima T, Delbecq M R, Allison G, Honda T, Kodera T, Oda S, Hoshi Y, Usami N, Itoh K M and Tarucha S 2018 *Nat. Nanotechnol.* **13** 102
[28] Petta J R, Johnson A C, Taylor J M, Laird E A, Yacoby A, Lukin M D, Marcus C M, Hanson M P and Gossard A C 2005 *Science* **309** 2180
[29] Hendrickx N W, Franke D P, Sammak A, Scappucci G and Veldhorst M 2020 *Nature* **577** 487
[30] Yang C H, Leon R C C, Hwang J C C, Saraiva A, Tanttu T, Huang W, Camirand L J, Chan K W, Tan K Y, Hudson F E, Itoh K M, Morello A, Pioro-Ladrière M, Laucht A and Dzurak A S 2020 *Nature* **580** 350
[31] Mills A R, Guinn C R, Gullans M J, Sigillito A J, Feldman M M, Nielsen E and Petta J R 2022 *Sci. Adv.* **8** abn5130
[32] Xue X, Russ M, Samkharadze N, Undseth B, Sammak A, Scappucci G and Vandersypen L M 2022 *Nature* **601** 343
[33] Noiri A, Takeda K, Nakajima T, Kobayashi T, Sammak A, Scappucci G and Tarucha S 2022 *Nature* **601** 338
[34] Bloch F and Siegert A 1940 *Phys. Rev.* **57** 522
[35] Zhang T, Liu H, Gao F, Xu G, Wang K, Zhang X, Cao G, Wang T, Zhang J, Hu X, Li H O and Guo G P 2021 *Nano Lett.* **21** 3835
[36] Liu H, Zhang T, Wang K, Gao F, Xu G, Zhang X, Li S X, Cao G, Wang T, Zhang J, Hu X, Li H O and Guo G P 2022 *Phys. Rev. Appl.* **17** 044052
[37] Xu G, Li Y, Gao F, Li H O, Liu H, Wang K, Cao G, Wang T, Zhang J J, Guo G C and Guo G P 2020 *New J. Phys.* **22** 083068
[38] Winkler R 2003 *Spin–orbit Coupling Effects in Two-Dimensional Electron and Hole Systems* vol. 191 (Heidelberg: Springer Berlin)
[39] Bravyi S, DiVincenzo D P and Loss D 2011 *Ann. Phys.* **326** 2793
[40] Rahav S, Gilary I and Fishman S 2003 *Phys. Rev. A* **68** 013820
[41] Goldman N and Dalibard J 2014 *Phys. Rev. X* **4** 031027
[42] Zhou Y, Gu S, Wang K, Cao G, Hu X, Gong M, Guo G C, Li H O and Guo G P 2023 *Phys. Rev. Appl.* **19** 044053
[43] Shirley J H 1965 *Phys. Rev.* **138** B979
[44] Zajac D M, Sigillito A J, Russ M, Borjans F, Taylor J M, Burkard G and Petta J R 2018 *Science* **359** 439
[45] Petersson K D, Petta J R, Lu H and Gossard A C 2010 *Phys. Rev. Lett.* **105** 246804
[46] Dial O E, Shulman M D, Harvey S P, Bluhm H, Umansky V and Yacoby A 2013 *Phys. Rev. Lett.* **110** 146804